PERGAMON

Available online at www.sciencedirect.com
SCIENCE DIRECT®

International Journal of Multiphase Flow 29 (2003) 173–194

International Journal of Multiphase Flow

www.elsevier.com/locate/ijmulflow

Heat transfer to two-phase flow in inclined tubes

G. Hetsroni [a,*], D. Mewes [b], C. Enke [b], M. Gurevich [a], A. Mosyak [a], R. Rozenblit [a]

[a] *Faculty of Mechanical Engineering, Technion—Israel Institute of Technology, 32000 Haifa, Israel*
[b] *Institute for Process Engineering, University of Hannover, 30167 Hannover, Germany*

Received 14 August 2001; received in revised form 27 October 2002

Abstract

Experiments were performed to study the flow regimes and heat transfer in air–water flow in 8° inclined tubes of inner diameter of 49.2 and 25 mm. The flow regimes were investigated by using high-speed video technique and conductive tomography. The thermal patterns on the heated wall and local heat transfer coefficients were obtained by infrared thermography. Under the conditions studied, disturbance waves of different forms were observed. The analysis of the behavior of the heat transfer coefficients, together with flow visualization and conductive tomography showed that dryout took place in the open annular flow regimes with motionless or slowly moving droplets. Even under these conditions, the heat transfer coefficient is about 10 times higher than that for single-phase airflow.

Keywords: Heat transfer; Dryout; Two-phase flow; Annular flow; Cluster

1. Introduction

Today's parabolic trough solar power plants are based on a conventional Rankine steam cycle, which is heated via primary oil by concentrated solar radiation. In order to improve the efficiency of the cycle and to reduce the investment costs, it is planned to avoid the oil loop. The steam required to drive the turbine/generator unit will be produced directly in the absorber tubes of the solar field (DSG: direct steam generation). Similar two-phase flows are often encountered in a wide range of industrial applications: chemical plants, oil wells and pipelines, evaporators etc.

Flow patterns of the evaporating two-phase flow, in the absorber tubes, are of special interest since the tubes are inclined and, therefore, dryout may occur due to the influence of gravity at low

* Corresponding author. Tel: +972-4-8292058; fax: +972-4-8238101.
E-mail address: hetsroni@tx.technion.ac.il (G. Hetsroni).

0301-9322/03/$ - see front matter
PII: S0301-9322(02)00132-5

flow velocities. Temperature differences around the circumference of the pipe, resulting from large differences of the heat transfer coefficients in the case of dryout, may cause excessive thermal stress in the pipe material and/or damaging the selective paint on the tubes. Experiments on adiabatic air–water flow performed by Barnea and Taitel (1993), and experiments in diabatic air–water flow carried out by Mosyak and Hetsroni (1999) showed that the temperature difference between the top and the bottom was quite large for horizontal pipes. It drastically decreased due to an inclination of the pipe. However, outside the region of pure stratified flow, the flow will not change abruptly to close annular flow, but there exists a region where a liquid film at the top of the pipe is gradually built up, as observed in the present study. Because of their obvious importance, instabilities of thin films have been the subject of numerous studies, such as those of Wallis (1969), and Hewitt and Hall-Taylor (1970). The one-dimensional linear stability analysis of gas–liquid flow was presented by Lin and Hanratty (1986). Andritsos and Hanratty (1987) investigated the effect of interfacial instabilities in horizontal flow, which lead them to the determination of different types of waves. Such regimes were observed by Jurman et al. (1989) in the gas–liquid horizontal flow. Foukano and Ousaka (1989) proposed a model based on the pumping action of waves along the sides of the pipe. Smaller waves initialize droplet atomization and lead to droplet deposition on the pipe walls at higher gas and lower liquid superficial velocities. The equations of continuity and motion of gas and liquid were solved numerically by Barnea and Taitel (1993). The resulting stability criteria for interfacial waves were similar to those of Wallis (1969). A model for stability of wavy flow in inclined pipes was presented by Grolman et al. (1996). In this study the main parameter for predicting instability is the average liquid holdup. Flow-pattern maps were presented for selected angles of inclination, but superficial gas velocities did not exceed $U_{GS} = 30$ m/s. The effect of inclination on drop sizes in annular gas–liquid flow was studied by Azzopardi and Zaidi (1997). Creation of droplets was closely associated with the large amplitude waves, which formed on the surface of the film.

The flow pattern that exists in high sheared gas–water flow is characterized by intermittent appearance of aerated masses of liquid that travel downstream. These aerated masses are separated from one another by a configuration that contains a slower moving liquid layer.

In the present study the flow patterns occurring on the liquid, which is highly sheared by a gas flow, are investigated. Connection between flow parameters and heat transfer was also studied by IR thermography in diabatic air–water flow. Large difference of circumferential wall temperature was found in these experiments. In the open annular flow regime, there is no continuous liquid film on the upper part of the pipe, which results in a low heat transfer coefficient on that part. The hydrodynamic behavior and heat transfer was analyzed to get information on the connection between these processes.

2. Description of the experiments

2.1. Experimental apparatus

The experiments were conducted in two identical loops with a tube diameter of 49.2 and 25 mm, respectively, at upward inclination of 8°. A schematic diagram of the experimental facility is presented in Fig. 1. Water, at a constant temperature, was circulated from a tank (1) through the

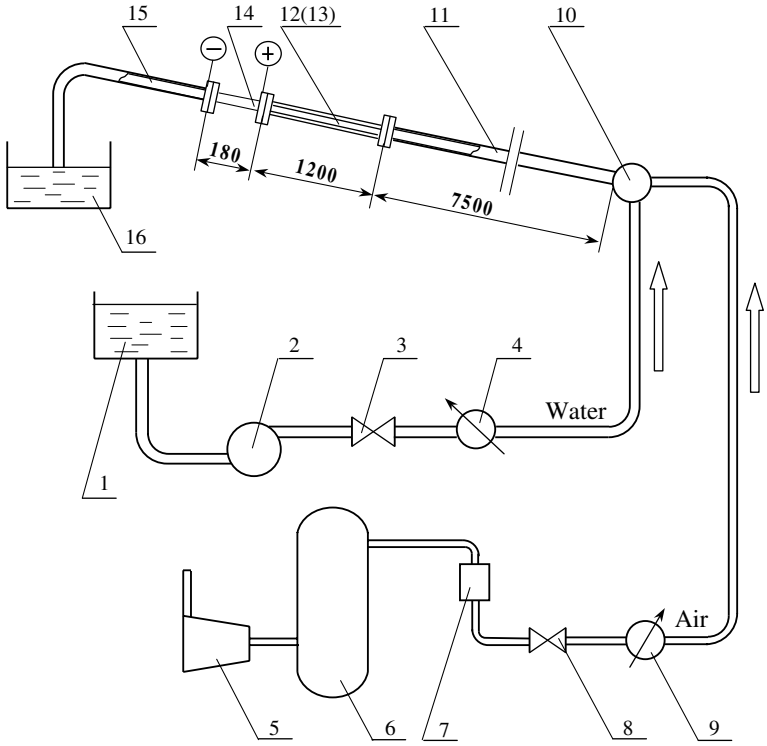

Fig. 1. Experimental facility: (1) entrance tank, (2) pump, (3) water flow regulator, (4) flowmeter, (5) compressor, (6) receiver, (7) filter, (8) air regulator, (9) air flowmeter, (10) mixing section, (11) flow development section, (12) glass section, (13) section of development of thermal boundary layer, (14) test section for temperature measurements and thermal pattern visualization, (15) exit section, (16) tank for water flow rate measurements.

loop by means of a pump (2). The liquid flow rate was regulated by a valve (3) and measured by a flow-meter (4). The air was delivered by compressor (5) through receiver (6) and filter (7). The air rate was regulated by valve (8) and measured by an air velocity transducer (9). After that the air and water were mixed in a mixing chamber (10). The 10.68 m long inclined smooth pipe consisted of four parts: the flow development section (11), the section of flow visualization (12), which could be replaced by heated thermal boundary layer section (13) (for measurements of the heat transfer), the heated test section (14) and the outlet section (15). The 7.5 m long development section (11), and the 1.8 m long outlet section (15) were made of plastic tube. In Fig. 2a and b two versions of the main part of the experimental setup are shown. The glass section for visual observation (2) is located between the development section and the heated test section (1). The high-speed video camera was used for recording hydrodynamic patterns in the inclined tube. The heated test section for studying heat transfer (180 mm long) (1) was constructed of a 0.05 mm thick stainless steel foil (6) rolled in the form of the tube with the same inner diameter. The foil stretching and electrical connection was provided with a special mechanism. The heating was achieved by supplying DC power up to 800 A. In the runs for heat transfer measurements, the section for flow visualization was replaced by the same length and diameter plastic tube with a heater (5). This heated section is shown in Fig. 2b. The same stainless steel foil, serving as a heater of the section (1), was attached

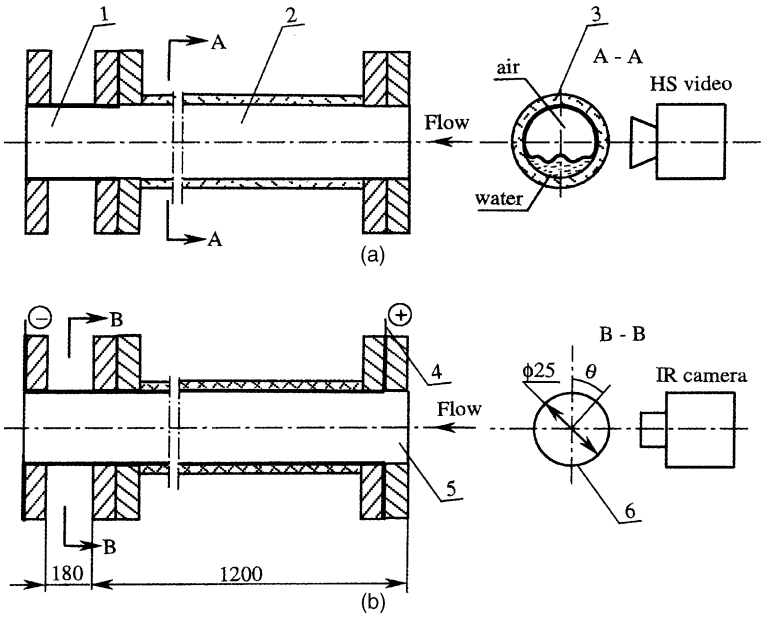

Fig. 2. Visualization of flow regimes and temperature patterns. (a) Device for flow regime visualization: (1) section for temperature measurements; (2) flow visualization section; (3) glass tube. (b) Device for thermal pattern visualization: (4) electrical contact; (5) section for development of thermal boundary layer; (6) heater made of stainless steel foil.

to the inner surface of this tube. It was done to obtain a developed thermal boundary layer before the test section (1). The thermal pattern visualization and heat transfer measurements were recorded by IR radiometer.

2.2. Measurement techniques

The hydrodynamic pattern in the pipes was studied by analyzing high-speed video images. The method is based on the detection of the edges of flow disturbance in a sequence of video frames. This method allows one to measure the water level, velocity and frequency of water disturbances. The motion of the disturbance in the annular flow was recorded by a high-speed motion analyzer, with recording rate up to 10,000 frames per second. The illumination was provided by a set of 500 W halogen lamps, mounted on a frame. Pictures were taken against a black background, so that the wave disturbances had a white outline. Each run a sequence of at least 120 s was recorded. In the playback mode, typical flow patterns were frozen on the TV monitor and analyzed frame by frame to calculate the average water level, propagation velocity and frequency for each set of the data.

An IR radiometer was used for investigating the thermal patterns. It has a typical horizontal and vertical resolution of 256 pixels per line. The radiometer gives a qualitative thermal profile in the "line mode", the average temperature in the "area mode", and the temperature of a given point in the "point mode". The experiments were carried out at a constant heat flux. We had to consider the frequency response of the system to changes in the heat transfer coefficient. It was

shown by Hetsroni and Rozenblit (1994) that temperature distortions and phase shift in temperature fluctuations on the heated wall begin at $f = 15$–$20\ s^{-1}$. In the present study the highest cluster frequency was higher, so that we confined our measurements to average temperatures and qualitative observation of the thermal structure on the heated wall. The average surface temperature was measured with an accuracy of ± 0.1 °C. The air and water flow rates were measured with an accuracy of 2%. Electrical power was determined by means of a digital wattmeter with an accuracy of 1%.

The flow patterns in highly sheared air–water flow were investigated using conductive tomography. The use of this method allowed to distinguish between the flow patterns of open and closed annular flows and to determine the liquid film thickness with an accuracy of 0.01 mm at different positions around the pipe circumference. The electrodes are installed flush with the inner pipe surface. The measurement is based on a change of resistance in an electrical field when liquid film passes the electrodes. The smallest measurement value of voltage, which can be evaluated by calibration data, corresponds to film thickness of 0.01 mm. Since for film thickness less than 0.01 mm the calibration could not be performed properly, we assumed that in the region of 0–0.01 mm the voltage varied linearly.

2.2.1. Single-phase tests

A number of verification runs were done prior to the data logging. A series of single-phase air tests were made to establish the validity of the system and testing the technique. Preliminary calculations presented by Hetsroni and Rozenblit (1994) have shown that the difference between the temperature of the two sides of the thin (0.05 mm) foil, was less than 0.1 K. The axial heat conduction for the heated test section was calculated by using measurements of wall temperature distribution in the streamwise direction. The heat transfer in the axial direction was less than 0.5% of that in the radial one. Heat balance for the variation of the outside ambient temperature has also been verified by direct measurements. The estimated total heat losses were in the range of 3–4%, depending on the values of the heat flux.

The space and time-averaged heat transfer coefficient in the single-phase air flow is defined as

$$\alpha_0 = q/(T_w - T_f) \tag{1}$$

where q is the heat flux, T_w is the averaged wall temperature, T_f is the bulk temperature of the fluid. The experimental results agreed well those calculated for a fully developed turbulent flow in the tube (Kays, 1966):

$$Nu = 0.022 Re^{0.8} Pr^{0.6} \tag{2}$$

2.2.2. Air–water flow

Our discussion is limited to the definition of heat transfer coefficient—because it is the averaging value for which the dryout must be specified. Since microscopic details of this process are rarely needed for engineering problems, the macroscopic nature of the process is usually much more important. The averaging operation effectively eliminates information on local instantaneous fluctuation. Eulerian averaging is of most interest in this study, because it involves averaging over time and space, which are the independent variables. In the present study we use

time-averaged value of the heat transfer coefficient at a fixed point located at an angle θ which is the angle from the top of the pipe:

$$\alpha_\theta = \frac{1}{\tau}\int_0^\tau \alpha(\tau)\,\mathrm{d}\tau \tag{3}$$

and time and space mean value, of heat transfer coefficient within the angle θ and $\theta + \Delta\theta$:

$$\alpha_{\Delta\theta} = \frac{1}{\tau\,\Delta\theta}\int_0^\tau \int_\theta^{\theta+\Delta\theta} \alpha(\tau,\theta)\,\mathrm{d}\tau\,\mathrm{d}\theta \tag{4}$$

If partial dryout is present in two-phase flow, the averaged heat transfer coefficient has contributions from both liquid and gas phases.

2.3. Experimental procedure

The water and air were mixed in a mixing chamber upstream of the test section. Two-phase tests were conducted at various liquid and air superficial velocities. The pump, compressor, and the power source were set and maintained at desired output. The output of the power source was set as to obtain desired temperature distribution on the heated test section. The experiments were repeated at least four times to confirm their reproducibility. The heat transfer and flow parameters for each data run were measured under steady-state conditions. At such a steady state, the temperatures, the flow rates and heating power were recorded for about 20 min.

Data reduction. Before presenting the experimental results, it is of interest to discuss briefly the dimensionless parameters used in the analysis. An application of the Buckingham Pi-theorem to the motion of air and water indicates that the following dimensionless groups can be found: $Fr_\mathrm{L} = U_\mathrm{LS}^2/gD$, $Fr_\mathrm{G} = U_\mathrm{GS}^2/gD$, H/D, $\rho_\mathrm{G}/\rho_\mathrm{L}$, $\mu_\mathrm{G}/\mu_\mathrm{L}$, $U_\mathrm{GS}/U_\mathrm{LS}$, U_C/U_LS, $\sigma\rho_\mathrm{L}D/\mu_\mathrm{L}^2$, $Re_\mathrm{L} = U_\mathrm{LS}D\rho_\mathrm{L}/\mu_\mathrm{L}$, $Re_\mathrm{G} = U_\mathrm{GS}D\rho_\mathrm{G}/\mu_\mathrm{G}$, α/α_0, where D is the pipe diameter; H, the height of air–water cluster; ρ_G, ρ_L and μ_G, μ_L, the density and viscosity of the gas and the liquid, respectively; U_LS and U_GS, superficial liquid and gas velocities, respectively; U_C, the velocity of the air–water cluster; σ, the surface tension; g, the acceleration due to gravity; α, the heat transfer coefficient in air–water flow; α_0, the heat transfer coefficient in air (gas single phase). Fr_L and Fr_G are liquid and gas Froude numbers, Re_L and Re_G are liquid and gas Reynolds numbers, respectively.

The data are usually correlated in a two-dimensional map using U_LS–U_GS coordinate system. Indeed, the ratio of Froude numbers $Fr_\mathrm{L}/Fr_\mathrm{G}$ and the ratio of Reynolds numbers $Re_\mathrm{L}/Re_\mathrm{G}$ can be easily converted to the velocity ratios by use of the viscosity and density rations. In this case the given flow pattern could be predicted by one map for pipes with different inner diameters. Unfortunately, this is seldom the case and, generally, the usefulness of such predictive scheme is doubtful. The majority of the data reported on flow pattern transitions have dealt with either horizontal or vertical tubes with only limited results reported for inclined pipes. Several investigators performed experiments only for tube with one inner diameter. The results reported by Spedding and Nguyen (1980) are based on data collected in a pipe with an inner diameter of 4.55 cm. Barnea et al. (1985) reported data on flow pattern transition in gas–liquid flow in upward inclined pipes with inner diameter of 2.55 and 5.1 cm. The flow pattern maps are different, depending on the inner diameter of the pipe. The transition to annular flow was found (Lin and Hanratty, 1987) to occur by means of mechanisms, which depend upon pipe diameter. Annular

flow was found to develop at lower gas velocities by a mechanism of wave wrapping in 2.52 cm (i.d.) pipeline, compared to an annular flow droplet deposition mechanism in 9.53 cm (i.d.) pipeline. Spedding et al. (1998) used Froude number to present flow pattern map of air–water data for 5.08 m (i.d.) pipe at inclination of +5°.

We assume that the surface tension is constant, and that the value of the heat transfer coefficient was measured at constant Prandtl number. For this reason, all the experiments were performed with the heated surface at wall temperature was not higher than 20 K above the mean temperature of the fluid.

It is clear that in the analysis we do not use all dimensionless groups from above. The method of choice is based on the physical analysis of the phenomenon and on the reasonable guess of the "important" dimensionless groups that allow one to describe experimental data by a common curve.

In the majority of two-phase heat transfer correlations the transport properties of the fluids are related to average (at the inlet and the outlet of the test section) temperature. We used dimensionless parameters Re_G and Fr_L to present experimental data. The difference between wall and flow temperatures did not exceed 20 K. Under these conditions the variance of Re_G is less than 3%.

3. Results

3.1. Flow regimes

3.1.1. Flow in a 49.2 mm pipe (visual observations)

The purpose of these experiments was to characterize different flow details under conditions when the superficial gas velocity is constant and the superficial liquid velocity increases. The upward flow regimes are presented in Fig. 3. Fig. 3a shows the flow pattern at $U_{GS} = 20$ m/s and $U_{LS} = 0.005$ m/s. In the region of pure stratified flow the liquid layer is drawn upward by the gas via the interfacial shear stress. No droplets could be observed at the interface. Such a regime was also observed by Taitel and Dukler (1976) and Spedding et al. (1998).

Droplets appeared on the surface of the pipe (Fig. 3b) after increasing the water flow rate up to $U_{LS} = 0.007$ m/s. Spedding et al. (1998) referred this regime to "film plus droplet pattern". When the water flow rate increased and superficial liquid velocity was $U_{LS} = 0.03$ m/s, droplets began to roll back into the liquid film. Kokal and Stanislav (1989) identified such a regime as "annular plus roll wave flow pattern". The experimental facility used in the present study allowed us to achieve values of superficial gas velocities up to 20 m/s in the 49.2 mm pipe. Therefore, to study the flow regimes at higher superficial gas velocities the pipe diameter was decreased.

3.1.2. Flow in a 25 mm pipe (visual observations)

The second part of the experiments was carried out in a pipe of inner diameter 25 mm. The experiments were carried out in the range of the $U_{LS} = 0.016$–0.17 m/s and $U_{GS} = 24$–55 m/s.

Experimental investigations in the 25 mm pipe reveal significant differences from the results obtained in the 49.2 mm pipe. Fig. 4 shows an instantaneous side view of air–water flow into the tube, obtained by high-speed video camera. The flow moves from right to left. The distance in the

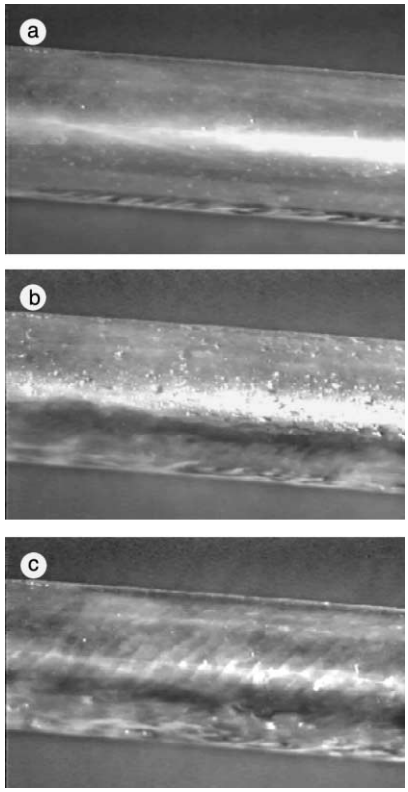

Fig. 3. Flow pattern in the pipe 49.2 mm, $U_{GS} = 20$ m/s. (a) $U_{LS} = 0.005$ m/s; (b) $U_{LS} = 0.007$ m/s; (c) $U_{LS} = 0.03$ m/s.

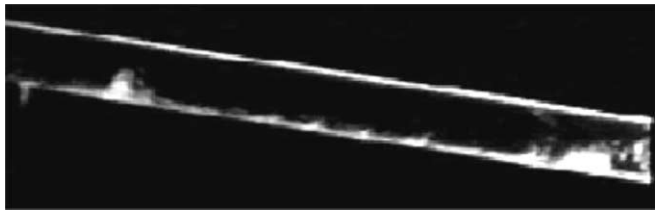

Fig. 4. Annular flow in the pipe 25 mm with air–water clusters.

flow direction is 280 mm. The picture was captured at following values of the superficial velocities $U_{GS} = 36$ m/s and $U_{LS} = 0.045$ m/s. The light regions on the left and right side of the image are air–water clusters, the smooth light bands reflect the disturbance wave flow at the lower part of the tube and liquid film at the upper part of the tube, respectively.

It was observed that as some new waves were created, others disappeared. This process occurred either by faster waves catching up with slower waves and engulfing them or occasionally by waves appearing to die spontaneously (an event, which apparently occurs when the amplitude of the disturbance wave got too large). In Fig. 4 one can distinguish the regions of disturbance wave

without air–water clusters and air–water clusters that occupied significant cross-section area. This flow pattern is difficult to identify since a problem existed in distinguishing visually between highly aerated slugs and wavy annular flow. This difficulty was overcome by the study of these patterns separately. Qualitative behavior of clusters showed that within a certain distance they propagated with some change in shape. Using high-speed video, it was possible to show separately the sequence of the frames with wave regimes and sequence of frames with air–water clusters.

Detailed typical instantaneous images of disturbance wave regions without air–water clusters are shown in Fig. 5a–d. The air–water clusters, also observed at these regions, are shown in Fig. 5e–h. Both sets of images were obtained at a superficial gas velocity $U_{GS} = 36$ m/s. The superficial liquid velocity varied form $U_{LS} = 0.016$ (Fig. 5a and e) to $U_{LS} = 0.17$ (Fig. 5d and h). The flow moves from right to left, the distance in the streamwise direction, shown in those figures, is about two tube diameters. Fig. 5a ($U_{LS} = 0.016$ m/s) shows open annular flow with disturbance waves. Fig. 5e shows rather small air–water clusters that some time were observed instead the flow

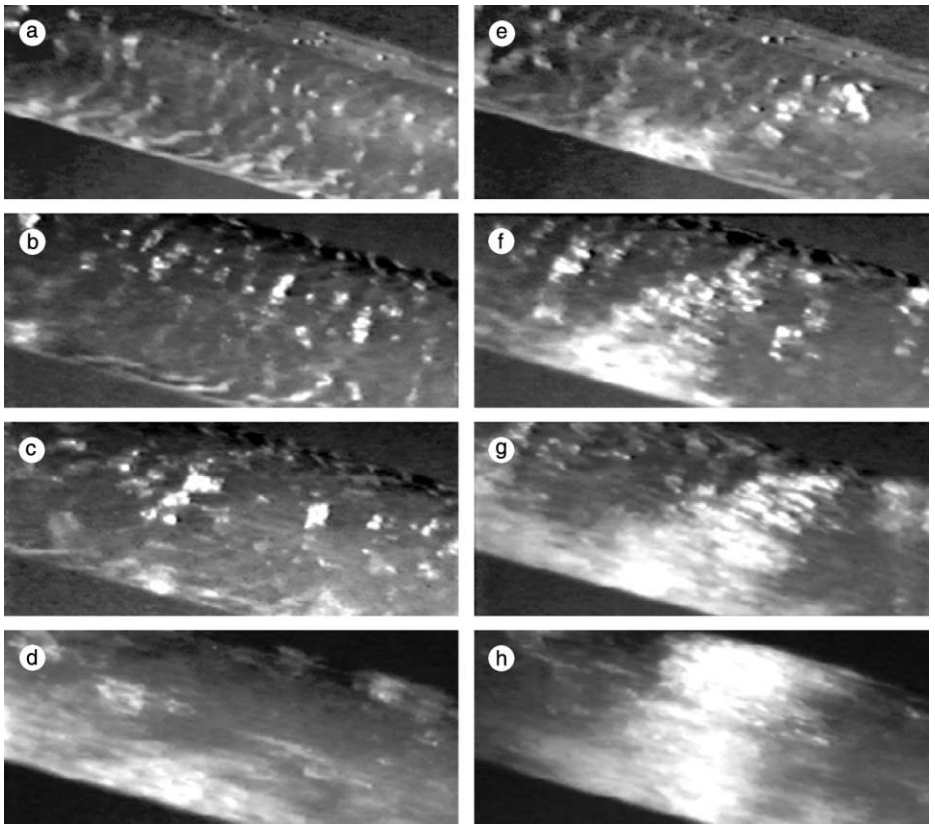

Fig. 5. Flow regimes in the pipe 25 mm at $U_{GS} = 36$ m/s. (a) $U_{LS} = 0.016$ m/s, disturbance waves with motionless droplets; (b) $U_{LS} = 0.027$ m/s, disturbance waves with moving droplets; (c) $U_{LS} = 0.045$ m/s, disturbance waves and liquid film on the upper tube part; (d) $U_{LS} = 0.17$ m/s, disturbance air–water waves and liquid film on the upper tube part; (e) $U_{LS} = 0.016$ m/s, small air–water clusters; (f) $U_{LS} = 0.027$ m/s, air–water clusters; (g) $U_{LS} = 0.045$ m/s, huge air–water clusters; (h) $U_{LS} = 0.17$ m/s, huge air–water clusters that block the tube cross-section.

pattern shown in Fig. 5a. It was determined from visual observations that in this case the drops on the upper part of the pipe almost did not move. When the liquid flow rate increased, Fig. 5b and f ($U_{LS} = 0.027$ m/s) the drops on the upper part of the pipe began to move. Velocity of the displacement of droplets in the flow direction is of an order of magnitude less than the superficial liquid velocity. Further increase in the liquid flow rate, Fig. 5c and g ($U_{LS} = 0.045$ m/s), leads to closed annular flow with liquid film on the upper part of the tube, in addition to air–water clusters. Fig. 5d and h ($U_{LS} = 0.17$ m/s), show the closed annular flow with huge air–water clusters, that often block the tube cross-section. Visual observations showed that under flow conditions, of the last two flow regimes, dryout was not observed. Parameters of air–water clusters were obtained from histograms of velocity and amplitude distribution. Fig. 5e–h show typical images that were used to describe characteristics of clusters in statistical terms for air–water regimes. When the clusters blocked the entire pipe cross-section, they touched the top wall only momentarily. It is of interest to note that the picture of air–water clusters, for 2.5 cm pipe, resembles the "pseudo-slugs" described by Lin and Hanratty (1987).

3.1.3. Velocity and amplitude of air–water clusters

Fig. 6 shows the dependence of the velocities of air–water clusters on the gas Reynolds number. The time-averaged amplitude of the air–water clusters, H, was obtained by using flow visualization technique. Fig. 7 shows the average non-dimensional value of H/D vs. the gas Reynolds number Re_G. The superficial liquid velocity was $U_{LS} = 0.016$–0.17 m/s, consequently, the range of

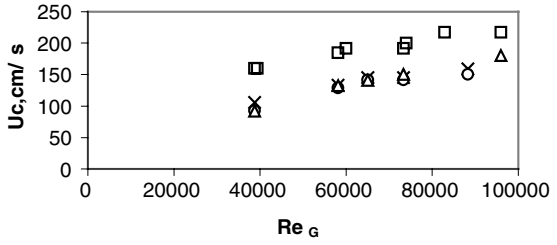

Fig. 6. Dependence of velocity of air–water clusters on gas Reynolds number (×) $U_{LS} = 0.016$ m/s, (○) $U_{LS} = 0.027$ m/s, (△) $U_{LS} = 0.045$ m/s, (□) $U_{LS} = 0.10$ m/s.

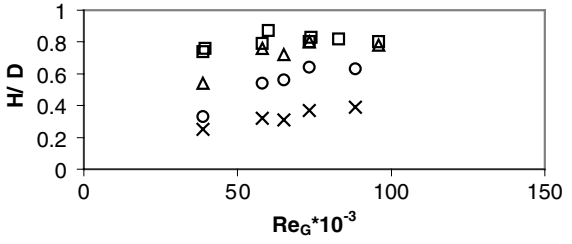

Fig. 7. Dimensionless time-averaged amplitude of air–water clusters vs. gas Reynolds number: (×) $Fr_L = 0.001$; (○) $Fr_L = 0.003$; (△) $Fr_L = 0.008$; (□) $Fr_L = 0.11$.

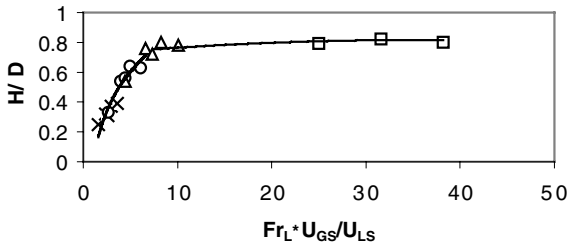

Fig. 8. Dependence H/D on $Fr_L U_{GS}/U_{LS}$. (×) $Fr_L = 0.001$; (○) $Fr_L = 0.003$; (△) $Fr_L = 0.008$; (□) $Fr_L = 0.11$.

liquid Froude number, Fr_L (based on the superficial liquid velocity and inner pipe diameter) varied from 0.001 to 0.11. For a given gas Reynolds number the ratio of H/D increases with an increase in Fr_L and reaches the value $H/D \approx 0.9$ at $Fr_L = 0.11$. In the range of Fr_L from 0.001 to 0.008 the value H/D increases with an increase in Re_G. Fig. 7 shows that at $Fr_L = 0.11$ the relation H/D is independent of the gas Reynolds number. This fact indicates that under these conditions the pipe diameter prevents formation of air–water clusters.

From Fig. 7 one can conclude that the gas Reynolds number Re_G, cannot be used solely to predict the behavior of U_C and H/D in a wide region of superficial flow velocities. At small liquid feeds, the values of Fr_L are small, but in inclined pipes much larger volumes of liquid are involved in gas–liquid clusters than in the actual transport of the liquid. The liquid holdup significantly depends also on Fr_L.

In Fig. 8 the value of H/D is presented vs. the parameter $Fr_L U_{GS}/U_{LS}$. From an analysis of the data presented in Fig. 8, one can conclude that the relation $Fr_L U_{GS}/U_{LS}$ is a useful parameter to describe the flow pattern of high sheared flows.

3.1.4. Film thickness

Figs. 9–12 show the results of film distribution around the circumference of the pipe. From Fig. 9 one can conclude that at $U_{LS} = 0.016$ m/s and $U_{GS} = 24$ m/s and $U_{GS} = 36$ m/s ($Fr_L U_{GS}/U_{LS}$ are 1.5 and 2.4, respectively) open annular flow occurs. Fig. 10 shows that at $U_{LS} = 0.027$ m/s and $U_{GS} = 24$ m/s ($Fr_L U_{GS}/U_{LS}$ is 2.66) also open annular flow occurs. These findings agree quite well with visual observations in the present study, and the top of the pipe is partially dry.

For pipe of 2.5 cm the flow patterns observed agree with the data reported by Lin and Hanratty (1987) for air and water flowing in horizontal 2.54 cm pipe. According to the flow regime map presented by Lin and Hanratty (1987) at $U_{LS} = 0.016$ m/s and $U_{GS} = 24$ m/s and $U_{GS} = 36$ m/s and at $U_{LS} = 0.027$ m/s and $U_{GS} = 24$ m/s the wavy stratified regime takes place. Results of flow visualization for the pipe of 4.92 cm agree with the flow map presented by Brauner and Moalem Maron (1992) for air–water flow in the pipe 5.1 cm. Barnea (1987) showed that small changes in the angle of inclination have a major effect on the stratified smooth-stratified wavy transition boundary. In the present study we consider stratified wavy-annular transition. In this case, as shown by Barnea (1987), transition boundaries do not change significantly within inclination angle +1 to +30°. That is why we believe that the parameter $Fr_L U_{GS}/U_{LS}$ is also useful for upward angle of inclination from +1 to +30°.

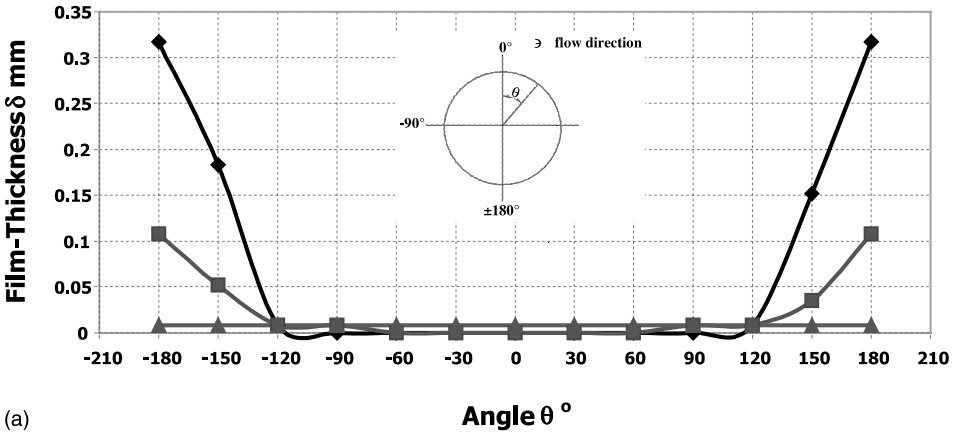

(a)

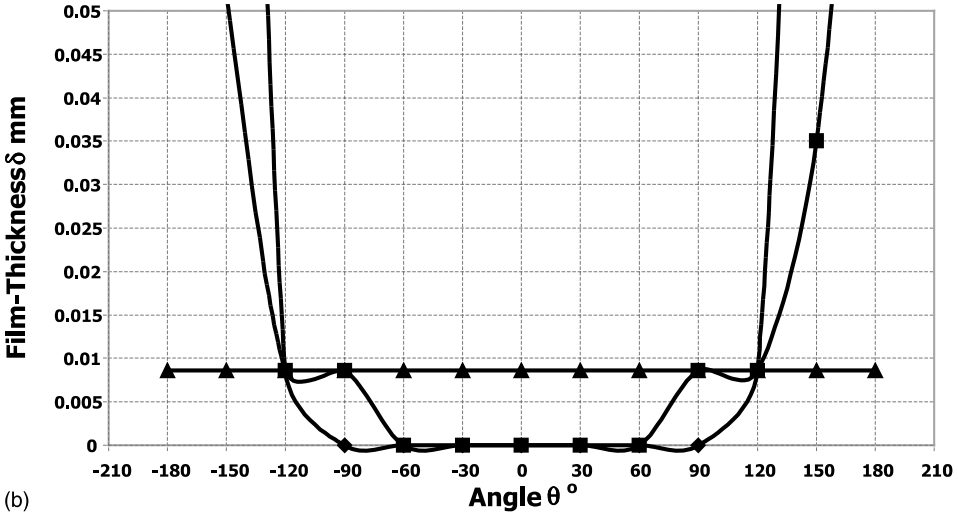

(b)

Fig. 9. Film-thickness distribution around circumference of the pipe at $U_{LS} = 0.016$ m/s: (a) full range; (b) zoom near the upper point of the pipe. U_{GS}: (◆) 24 m/s, (■) 36 m/s, (▲) 42 m/s.

3.1.5. Dryout

It is well known that at high gas flow rates significant amounts of liquid may be transported as drops entrained into the gas. We have also observed that gas may be similarly entrained and carried as clusters in the liquid layer. The effect on the gas is opposite to that of drop entrainment on the liquid, namely, the transport efficiency of the gas is low due to the generally slower moving fluid. As a result, the liquid layer puffs up and occupies a much larger area fraction of the pipe. Flow visualization showed that aerated high gas velocity pipe flow appears to consist of two distinct phases: an upper region consisting primarily of droplets and a lower region in which the liquid film and large air–water agglomerations moved. This phenomenon is similar to self-aerated flows in spillways. Under such conditions for pipe flow, dryout takes place. It is very difficult to predict theoretically dryout in such complex two-phase flow.

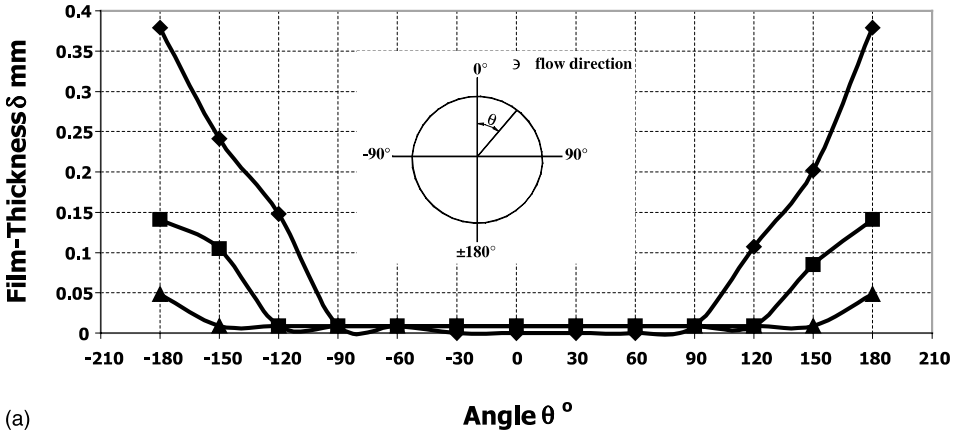

(a)

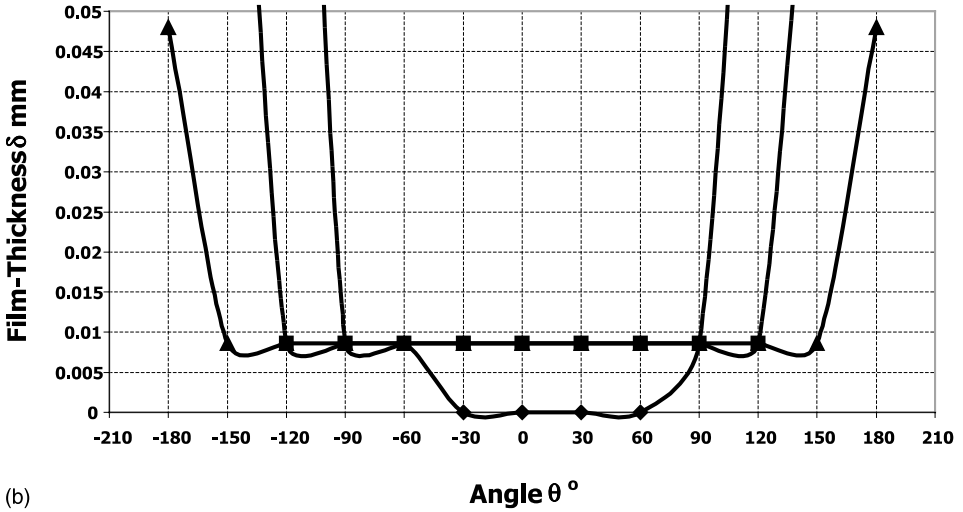

(b)

Fig. 10. Film-thickness distribution around circumference of the pipe at $U_{LS} = 0.027$ m/s: (a) full range; (b) zoom near the upper point of the pipe. U_{GS}: (◆) 24 m/s, (■) 36 m/s, (▲) 42 m/s.

We have performed experiments to measure the part of the wetted surface. This was done using a careful video record of the flow. We were not interested in the state of the flow at a specific instant in time, i.e. a single video frame, but in the average state over a period of time. In Fig. 13 the dimensionless angle, θ/π, is plotted vs. $Fr_L U_{GS}/U_{LS}$. In this Figure θ is the angle of the pipe, where the liquid film approaches zero. At $Fr_L U_{GS}/U_{LS} \geqslant 2.7$ the onset of closed annular flow takes place $\theta/\pi = 0$. The top of the pipe was never dry in that case. In the range of $Fr_L U_{GS}/U_{LS} \leqslant 2.7$ the experimental data are described by

$$\theta/\pi = 0.13(Fr_L U_{GS}/U_{LS})^{-1.3} \tag{5}$$

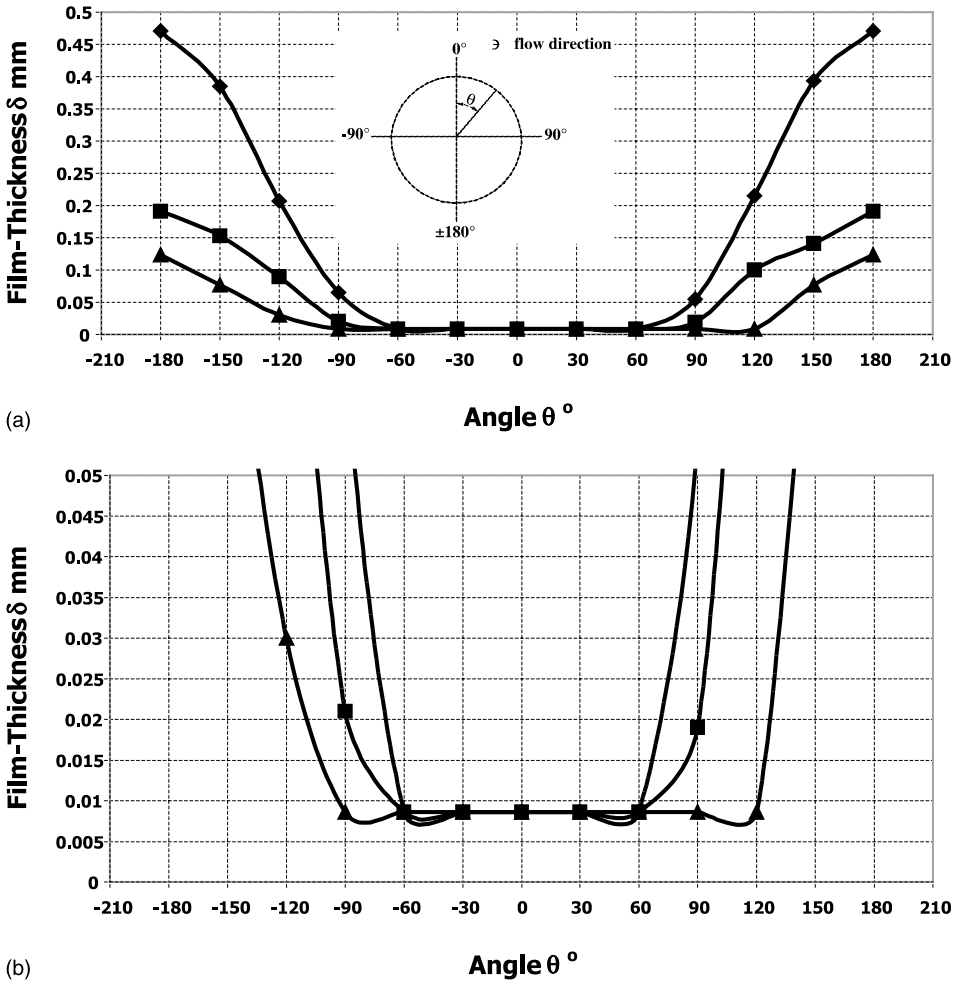

Fig. 11. Film-thickness distribution around circumference of the pipe at $U_{LS} = 0.045$ m/s: (a) full range; (b) zoom near the upper point of the pipe. U_{GS}: (◆) 24 m/s, (■) 36 m/s, (▲) 42 m/s.

3.2. Heat transfer

3.2.1. The 49.2 mm ID pipe

The local heat transfer coefficients on the surfaceof the pipe may not be uniform, though the surface is heated by uniform heat flux. This irregularity is due to the distribution of the air and liquid phase in the pipe. The temperature distribution along the pipe perimeter shows a maximum at the top and a minimum at the bottom of the pipe. Due to this temperature distribution part of the heat supplied at the top is conducted to the bottom. In the present study, since the wall of the heated part of the pipe was constructed of 0.05 mm foil, the tangential heat conduction was negligible. The local heat transfer coefficients were calculated from measured wall temperatures along the circumference of the pipe. The flow patterns observed in the 49.2 mm ID pipe are shown

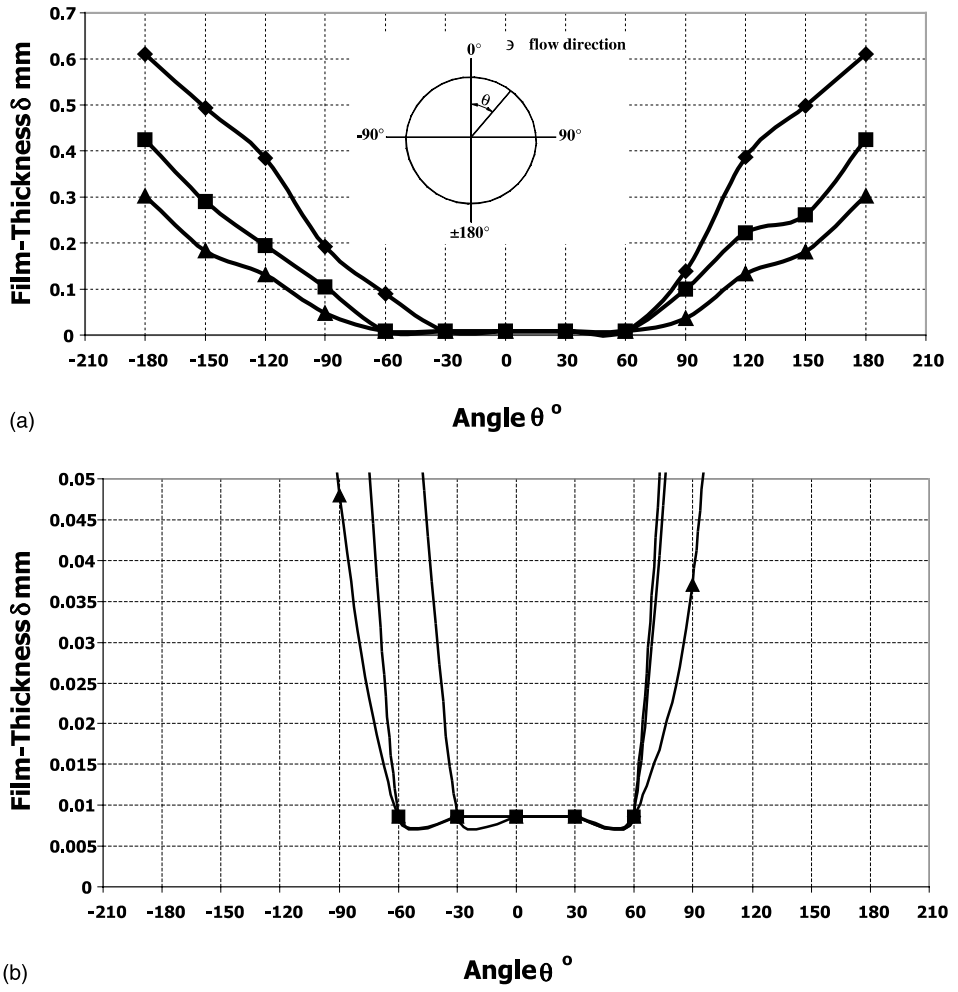

Fig. 12. Film-thickness distribution around circumference of the pipe at $U_{LS} = 0.099$ m/s: (a) full range; (b) zoom near the upper point of the pipe. U_{GS}: (◆) 24 m/s, (■) 36 m/s, (▲) 42 m/s.

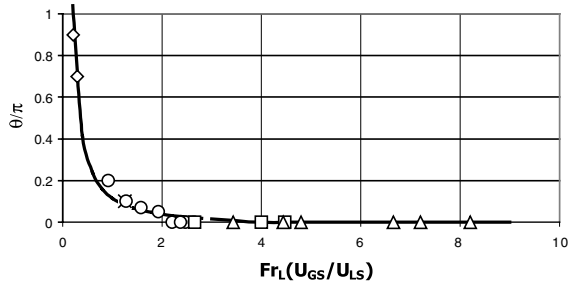

Fig. 13. Dimensionless angle θ/π vs. $Fr_L U_{GS}/U_{LS}$ (◇) $U_{LS} = 0.005$–0.007 m/s ($d = 49.2$ mm), (×) $U_{LS} = 0.03$ m/s ($d = 49.2$ mm), (○) $U_{LS} = 0.013$–0.016 m/s, (□) $U_{LS} = 0.027$ m/s, (△) $U_{LS} = 0.045$–0.0486 m/s.

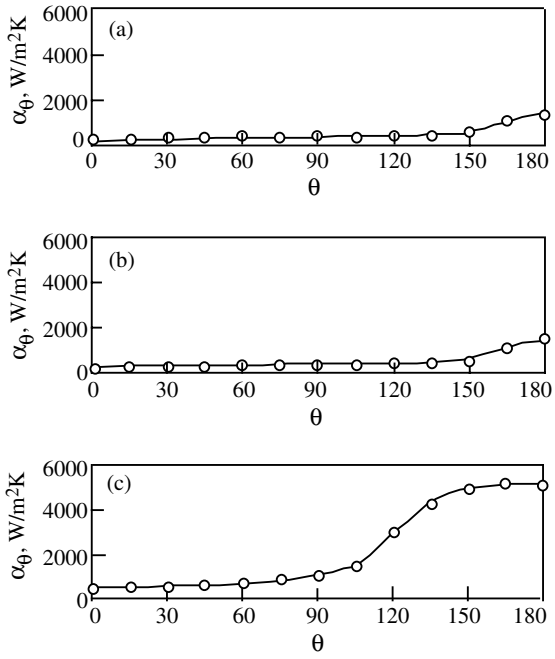

Fig. 14. Pipe 49.2 mm. $U_{GS} = 20$ m/s local heat transfer coefficients: (a) $U_{LS} = 0.005$ m/s, (b) $U_{LS} = 0.007$ m/s, (c) $U_{LS} = 0.03$ m/s.

in Fig. 3a–c, can be expected to yield large circumferential variation of the heat transfer coefficients. In Fig. 14a–c, the heat transfer coefficients α_θ are plotted vs. angle θ. These results were compared to simultaneous visual observations of the flow patterns. The distributions of α_θ plotted in Fig. 14a–c correspond to conditions under which the dryout of the upper part takes place.

3.2.2. The 25 mm ID pipe

Fig. 15a–d illustrate a typical temperature distribution in the range of the angle $0 \leqslant \theta < 180°$ (where $\theta = 0°$ is at the top of the tube). The heat flux was $q = 8000$ W/m^2, the superficial gas velocity was $U_{GS} = 36$ m/s. The superficial liquid velocities were 0.016, 0.027, 0.045 and 0.1 m/s, respectively. The flow moves from the right to the left. The color shades are indicative of the wall temperature. Comparison to simultaneous visual observations shows that the distribution of heat transfer coefficient at $U_{LS} = 0.016$ m/s corresponds to dryout on the upper part of the pipe.

The studies of the effect of numerous factors on dryout in flow boiling were performed by Hewitt and Wallis (1974), Elias and Yadigaroglu (1977). Chan and Banerjee (1981) and Nelson and Pasamehmetoglu (1992) presented a summary of the most significant analytical and numerical quasi-steady-state models. The important reason for the quasi-steady-state approach arises from the difficulty in obtaining a solution to the transient convection problem for the two-phase situations. In general, the term dryout indicates a local continuous contact of the gas phase with the surface. This term contains no statement as to the average (either spatial or temporal) value of the surface temperature at which dryout may occur. The term used in the present study is

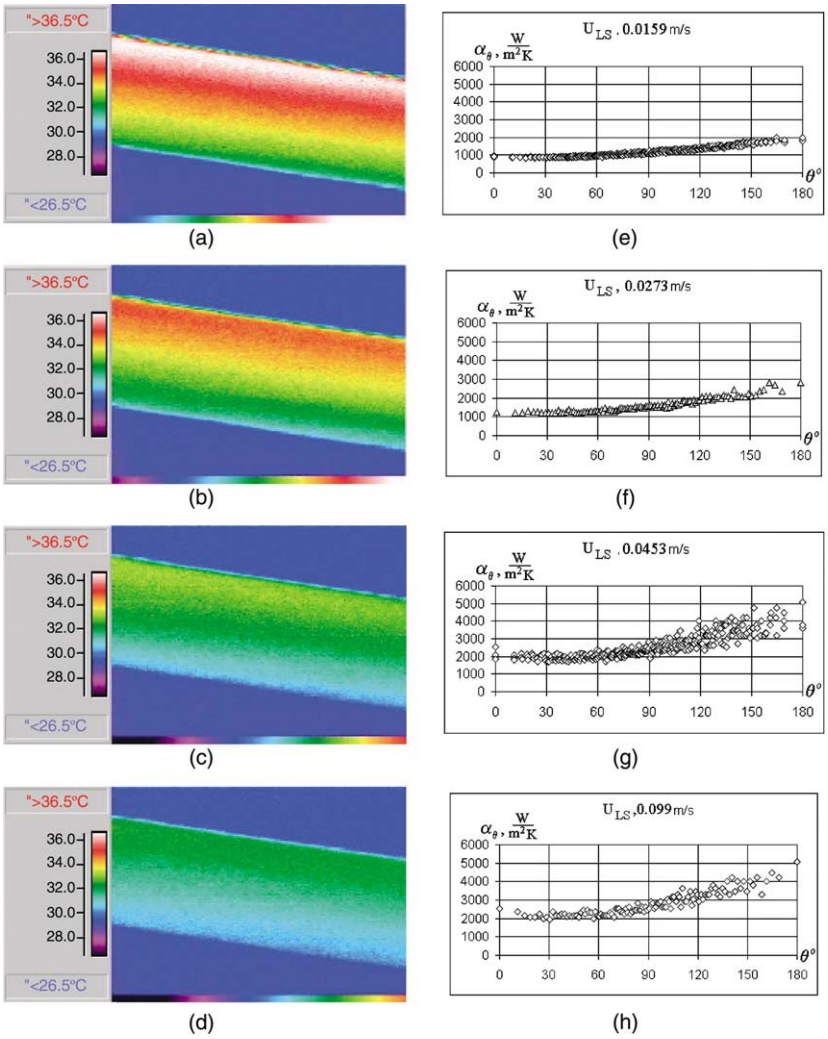

Fig. 15. Thermal patterns on the heated wall and local heat transfer coefficients, $U_{GS} = 36$ m/s, $q = 8000$ W/m^2. Thermal patterns: (a) $U_{LS} = 0.016$ m/s; (b) $U_{LS} = 0.027$ m/s; (c) $U_{LS} = 0.045$ m/s; (d) $U_{LS} = 0.099$ m/s. Local heat transfer coefficient: (e) $U_{LS} = 0.016$ m/s; (f) $U_{LS} = 0.027$ m/s; (g) $U_{LS} = 0.045$ m/s; (h) $U_{LS} = 0.099$ m/s.

defined with respect to averaged viewpoint of the process time. We assume that dryout may be detected using dimensionless parameter $\alpha_{\theta=0}/\alpha_G$, where α_G is the heat transfer coefficient in the single-phase airflow at the mean gas velocity $U = U_{GS}$.

Analysis of experimental data showed that the variation of the dimensionless heat transfer coefficient on the upper part of the pipe, $0 \leqslant \theta \leqslant \pi/2$, depends on the parameter $Fr_L U_{GS}/U_{LS}$. As it is seen from Figs. 9–12, in this range the film thickness did not exceed the value of 0.01 mm. In Fig. 16, the ratio $\alpha_{\theta=0}/\alpha_G$ of the heat transfer coefficient in a two-phase flow to that in single-phase (gas) flow at $\theta = 0$ is plotted vs. the value $Fr_L U_{GS}/U_{LS}$. The experimental data may be described by the equation:

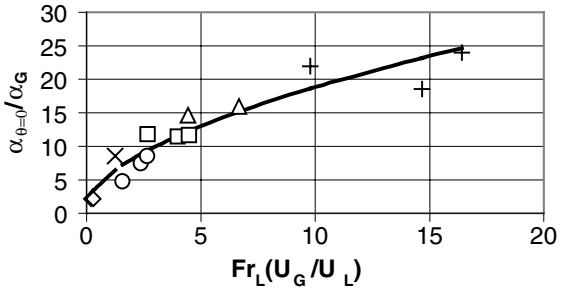

Fig. 16. Dimensionless heat transfer coefficient on the top of pipe: (◇) $U_{LS} = 0.005$–0.007 m/s ($d = 49.2$ mm), (×) $U_{LS} = 0.03$ m/s ($d = 49.2$ mm), (○) $U_{LS} = 0.013$–0.016 m/s, (□) $U_{LS} = 0.027$ m/s, (△) $U_{LS} = 0.045$–0.0486 m/s, (+) $U_{LS} = 0.099$ m/s.

$$\left(\frac{\alpha}{\alpha_G}\right)_{\theta=0} = 1 + 4.8(Fr_L U_{GS}/U_{LS})^{0.57} \tag{6}$$

At the dryout location, (flow parameter $Fr_L U_{GS}/U_{LS} < 2.7$) established from flow visualization and measurements of film thickness, liquid film was not observed on the wall. It was unexpected that the heat transfer coefficient did not drop dramatically. Depending on the flow parameter it is about 2.5–8 times higher, than that in air single-phase flow. The chief uncertainty of this conclusion is the definition of "dryout" in the present experiments. Although under certain flow conditions a complete liquid annulus is not formed at high enough gas velocities atomization of the liquid occurs and the top of the pipe can be partially wetted by droplets or liquid streaks. There could also be some very small droplets in the gas phase, which increase effective heat capacity. Fig. 17a–c show experimental data for angle $\theta = 30°$, 60° and 90°, respectively. The following equation describes the experimental data with standard deviation of 18%:

$$\alpha_\theta = \alpha_\pi - (\alpha_{\theta=\pi} - \alpha_{\theta=0})(1 - \theta/\pi)^{0.4} \tag{7}$$

where

$$\frac{\alpha_{\theta=0}}{\alpha_G} = 3050(U_{GS}/U_{LS})^{-0.56} \tag{8}$$

4. Discussion

4.1. Flow pattern

Before discussing the results it is instructive to consider the interrelation of these data to those previously published. Many studies were performed in the gas–liquid two-phase flow at moderate velocities of gas ($U_{GS} \leqslant 5$ m/s). Under these conditions the liquid lumps such as liquid slugs, huge waves and disturbance waves, were observed by Hewitt and Hall-Taylor (1970). In experiments performed by Azzopardi and Zaidi (1997) the superficial gas velocity was in the range of

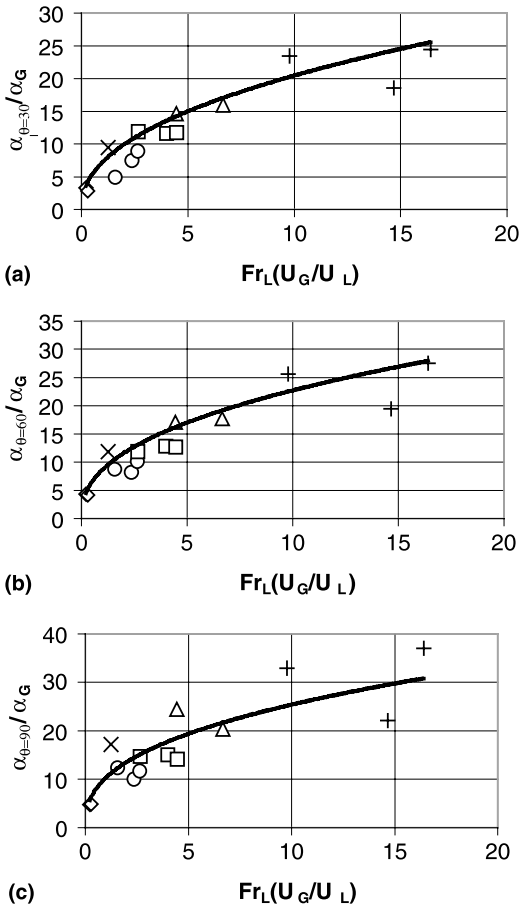

Fig. 17. Dimensionless heat transfer coefficient on the upper part of the pipe: (a) $\theta = 30°$; (b) $\theta = 60°$; (c) $\theta = 90°$. (◇) $U_{LS} = 0.005$–0.007 m/s ($d = 49.2$ mm), (×) $U_{LS} = 0.03$ m/s ($d = 49.2$ mm), (○) $U_{LS} = 0.013$–0.016 m/s, (□) $U_{LS} = 0.027$ m/s, (△) $U_{LS} = 0.045$–0.0486 m/s, (+) $U_{LS} = 0.099$ m/s.

$U_{GS} = 15$–30 m/s. An examination of flow pattern maps performed by those authors revealed that most of the data are from the stratified-atomization flow pattern. It can be noted that the increase in superficial gas velocity significantly affects flow regimes.

The following flow regimes were observed in the present study:

1. open annular flow with disturbance waves, small air–water clusters and stationary droplets;
2. open annular with air–water clusters and moving droplets;
3. closed annular with huge air–water clusters and liquid film on the upper part of the tube;
4. closed annular with huge air–water clusters that often block the tube cross-section.

As it was established from flow visualization experiments, the dryout takes place at regimes (1) and (2). It is an experimental fact that in wavy gas–liquid flow the core of turbulently flowing gas contains liquid in the form of droplets, liquid creeps up on the inner sides of the pipe to various

heights. Although this effect is rarely taken into account in the literature, it significantly affects the heat transfer coefficient. Hart et al. (1989) used the wetted wall fraction to calculate holdup in horizontal gas–liquid flow. For non-horizontal flow, the wetted wall fraction deviates considerably and systematically from the Hart et al. (1989) model. This model was modified by Grolman and Fortuin (1997), who presented the "modified apparent rough surface" model (MARS), which facilitates prediction of liquid holdup and pressure gradient in gas–liquid flow through horizontal and slightly sloping pipes. The calculated and measured results on both the liquid holdup and the pressure gradient are presented in the range $0 < U_{GS} < 12$ m/s and $U_{LS} = 0.0025$ m/s for a pipe of diameter $d = 26$ mm. The authors identified the flow regimes as slug and semi-slug flow. In our experiments the values U_{LS} were about 10 times higher ($0.016 < U_{LS} < 0.17$ m/s) and superficial gas velocity was varied in the range $24 < U_{GS} < 55$ m/s.

The process of wave formation and growth is quite different from that studied by Grolman and Fortuin (1997). The major phenomenon of the flow regimes is the air–water clusters that occupied a significant part of the cross-section. Under such circumstances much larger volumes of liquid are involved in oscillatory wave motion than in the actual transport of liquid. The behavior of such clusters should be taken into account to describe the governing physical processes for prediction of heat transfer.

The liquid layer depth plays an important role to predict behavior of stratified two-phase flow. Gangadharaiah et al. (1970) proposed an empirical correlation based on a liquid Froude number, which is based on the velocity and depth of the liquid layer. Lunde and Nuland (1997) used a hydraulic mean depth and liquid layer velocity. In our case the liquid layer was highly aerated and intermittent. Keeping in mind liquid deposits on the pipe wall above the liquid layer, drops in the gas, and air–water clusters we presented experimental data using the liquid Froude number based on superficial liquid velocity and pipe diameter. A liquid Froude number, which accounts for pipe diameter and superficial liquid velocity describe the flow parameters in the range of superficial flow velocity from $U_{LS} = 0.005$ to $U_{LS} = 0.17$ m/s, U_{GS} from 20 to 55 m/s, and heat transfer in the range $U_{LS} = 0.005$–0.1 m/s, $U_{GS} = 20$–55 m/s.

5. Conclusions

The following flow regimes were observed in the present study:

Open annular flow with disturbance waves; small air–water clusters and stationary droplets; open annular with air–water clusters and moving droplets; closed annular with huge air–water clusters and liquid film on the upper part of the tube; closed annular with huge air–water clusters that often block the tube cross-section.

The local heat transfer coefficients on the upper part of the pipe are described by empirical correlation with standard deviation of 18%.

The analysis of the heat transfer coefficients, together with flow visualization and film thickness measurements, showed that dryout may be associated with open annular flow with motionless or slowly moving droplets.

Under conditions of dryout in open annular air–water flow the heat transfer coefficient is about 2.5–8 times higher than that for single-phase airflow.

Acknowledgements

This research was supported by the Technion VPR Fund, and by the Niedersächsischen Ministerium für Wissenschaft and Kultur. M. Gurevich is partially supported by the Center for Absorption in Science, Ministry of Immigrant Absorption, State of Israel. A. Mosyak and R. Rozenblit are supported by a joint grant from the Center for Absorption in Science of Ministry of Immigrant Absorption and the Committee for Planning and Budgeting of the Council for Higher Education under the framework of the KAMEA PROGRAM.

References

Andritsos, N., Hanratty, T.J., 1987. Interfacial instabilities for horizontal gas–liquid flows in pipelines. Int. J. Multiphase Flow 13, 583–603.

Azzopardi, B.J., Zaidi, S.H., 1997. The effect of inclination on drop sizes in annular gas–liquid flow. In: Experimental Heat Transfer, Fluid Mechanics and Thermodynamics, M. Giot, F. Mayinger, G.P. Celata (Editors), Edizioni ETS, 1169-1176.

Barnea, D., 1987. A unified model for predicting flow pattern transitions for the whole range of pipe inclinations. Int. J. Multiphase Flow 13, 1–12.

Barnea, D., Shoham, O., Taitel, Y., Dukler, A.E., 1985. Gas liquid flow in inclined tubes: flow pattern transition for upward flow. Chem. Eng. Sci. 40, 131–136.

Barnea, D., Taitel, Y., 1993. Kelvin–Helmholtz stability criteria for stratified flow: viscous versus non-viscous (inviscid) approaches. Int. J. Multiphase Flow 19, 639–649.

Brauner, N., Moalem Maron, 1992. Analysis of stratified/non stratified transitional boundaries in inclined gas–liquid flows. Int. J. Multiphase flow 18, 541–557.

Chan, A.M.C., Banerjee, S., 1981. Refilling and rewetting of a hot horizontal tube, part 3: Application of a two-fluid model to analyze rewetting. Trans. ASME J. Heat Transfer 103, 653–659.

Elias, E., Yadigaroglu, G., 1977. A general one-dimensional model for conduction controlled rewetting of a surface. Nucl. Eng. Design 42, 185–194.

Foukano, T., Ousaka, A., 1989. Prediction of the circumferential distribution of film thickness in horizontal and near-horizontal gas–liquid annular flows. Int. J. Multiphase Flow 15, 403–419.

Gangadharaiah, T., Rao, N.S.L., Seetharamiah, K., 1970. Inception and entrainment in self-aerated flows. J. Hydraulics Division, ASCE, HY7 96, 1549–1565.

Grolman, E., Commandeur, N.C.J., De Baat, E.C., Fortuin, J.M.H., 1996. Wavy to slug flow transition in slightly inclined gas–liquid pipe-flow. AIChE Journal 42, 901–909.

Grolman, E., Fortuin, J.M.H., 1997. Liquid holdup, pressure gradient, and flow pattern in inclined gas–liquid pie flow. Experimental Thermal and Fluid Science 15, 174–182.

Hart, J., Hamersma, P.J., Fortuin, J.M.H., 1989. Correlations predicting frictional pressure drop and liquid-holdup during horizontal gas–liquid pipe flow with a small liquid hold up. Int. J. Multiphase Flow 15, 947–964.

Hetsroni, G., Rozenblit, R., 1994. Heat transfer to a liquid-solid mixture in a flume. Int. J. Multiphase flow 20, 671–689.

Hewitt, G.F., Hall-Taylor, N.S., 1970. Annular Two-Phase Flow. Pergamon Press, Oxford.

Hewitt, G.F., Wallis, G.B., 1974. Flooding and associated phenomena in falling flow in a vertical tube. ASME Winter Annual Meeting, Multiphase Flow Symposium, Philadelphia, PA.

Jurman, L.A., Bruno, K., McCready, M.J., 1989. Periodic and solitary waves on thin, horizontal, gas-sheared liquid films. Int. J. Multiphase Flow 15, 371–384.

Kays, W.M., 1966. Convective heat and mass transfer. McGraw-Hill Book Company, NY.

Kokal, S.L., Stanislav, J.F., 1989. An experimental study of two- phase flow in slightly inclined pipes, 1 Flow patterns, 2 Liquid hold-up and pressure drop. Chem. Eng. Sci. 44, 655–679, 681–693.

Lin, P.Y., Hanratty, T.J., 1987. The effect of pipe diameter on flow patterns for air–water flow in horizontal pipes. Int. J. Multiphase Flow 13, 549–563.

Lin, T.F., Hanratty, T.J., 1986. Prediction of the initiation of slugs with linear stability theory. Int. J. Multiphase Flow 13, 549–563.

Lunde, K., Nuland, S., 1997. Dispersed, stratified two-phase flow. In: Giot, M., Mayinger, F., Celata, G.P. (Eds.), Experimental Heat transfer, Fluid Mechanics and Thermodynamics, pp. 1145–1152.

Mosyak, A., Hetsroni, G., 1999. Analysis of dryout in horizontal and inclined tubes. Int. J. Multiphase Flow 25, 1521–1543.

Nelson, R.A., Pasamehmetoglu, K.O., 1992. Quenching Phenomena, In Post-Dryout Heat Transfer, Edited by G.F. Hewitt, J.M. Delhaye, N. Zuber, CRC Press, Boca Raton, Ann Arbor, London, Tokyo, 39–184.

Spedding, P.L., Nguyen, 1980. Regime maps for air–water two-phase flow. Chem. Eng. Sci. 35, 779–793.

Spedding, P.L., Watterson, J.K., Raghunathan, S.R., Ferguson, M.E.G., 1998. Two-phase co-current flow in inclined pipe. Int. J. Heat Mass Transfer 41, 4205–4228.

Taitel, Y., Dukler, A.E., 1976. A model for predicting flow regime transitions in horizontal and near-horizontal gas–liquid flow. AIChE J. 22, 47–56.

Wallis, G.B., 1969. One-dimensional two-phase flow. McGraw Hill, New York, Chapter 4.